

Angle-independent strain mapping in myocardial elastography

2D strain tensor characterization and principal component imaging

S. D. Fung-Kee-Fung, W.-N. Lee, C. M. Ingrassia, K. D. Costa and E. E. Konofagou
Department of Biomedical Engineering, Columbia University
New York City, New York, USA
ek2191@columbia.edu

Abstract—A current limitation of the implementation of myocardial elastography in a clinical setting is the difficulty of interpreting the one-dimensional strain maps due to varying strain values in the wall of the left ventricle (LV). In this paper, we demonstrate a robust angle-independent method for 2D myocardial elastography on simulated 2D ultrasonic images of a 3D finite-element analysis (FEA) model of the LV. Two FEA, a control and a regionally ischemic, canine left-ventricular models, were used and model states were obtained in increments and accumulated from end-diastole (ED) to end-systole (ES). Two-dimensional (2D) displacement in the myocardium was estimated between ED to ES. These estimates were good approximations of the FEA solution (rms errors of 0.18 mm for lateral displacement and 0.12 mm for axial displacement). The 2D symmetric strain tensor was calculated from the displacements and angle-independent principal strains were obtained using eigenvalue decomposition of the strain tensor. Principal strains in the myocardium have been shown to approximate normal strains with respect to an anatomical coordinate system [5]. To test this angle-independence, displacements were obtained from two different orthogonally placed transducer locations. Principal strains were estimated from both locations and showed good correlation to the FEA solution. Rms errors between the FEA model and 2D elastography (2DE) estimation of principal strains from both transducer locations were 1.7% and 2.4% strain, respectively. Visualizing the transmural strain using principal strains greatly simplified their interpretation. Moreover, abnormal deformation of the ischemic region, which was difficult to observe with axial and lateral strains, was clearly visible in the principal strain images. In summary, the feasibility of 2D elastography estimation of myocardial displacement and strain was shown. In this paper, we propose the use of principal strains as a more useful tool in the visualization of abnormal wall motion and the detection of ischemia and other related heart diseases.

Keywords: *angle-independent; eigenvalue; elastography; finite-element analysis; myocardial; principal strain*

I. INTRODUCTION

Current standards for the detection and measurement of ischemia and related heart diseases in clinical cardiology employ qualitative analysis of left ventricular (LV) wall motion and wall thickening using ultrasound. Recent studies have used ultrasound to quantify and study local mechanical properties, like strain, in the LV wall [1-3]. Konofagou et al. showed the feasibility of elastography (strain imaging) as a new method to

quantify and visualize abnormalities by estimating local displacements and strains in a healthy human heart in vivo [1].

Myocardial elastography [1] currently uses 1D axial strain (i.e. strain measured along the axis perpendicular to the face of the ultrasound transducer) to measure transmural strain since the resolution is far greater in the axial direction than in the lateral direction (parallel to the face of the transducer). However, axial strain maps are difficult to interpret as the values depend on the orientation of the imaging beam, relative to the ventricular wall. Axial strains in the anterior wall of the LV are vastly different from those in the posterior wall. Even though the motion is similar, the different directions of the motion change the values and complicate their interpretation.

One goal of this study was to build upon current techniques to estimate all strains within a two-dimensional (2D) ultrasound image. A method was proposed by Konofagou and Ophir [4] to image 2D deformations in vivo. Such a method would allow for the calculation of a 2D strain tensor which would characterize all (normal and shear) in-plane strains with respect to the axial and lateral axes. The 2D strain tensor would still suffer the same limitation as the 1D strain map. However, obtaining and mapping the 2D strain tensor, more specifically the 2D symmetric strain tensor, allows the calculation of the principal strain values which measure the local maximum and minimum in-plane strains independent of the transducer orientation. Principal strains in the myocardium have been shown to approximate the normal strains with respect to an anatomically-based coordinate system (i.e., radial, circumferential and longitudinal) [5].

Therefore, the main objective of this study was to show that by estimating 2D motion and characterizing the 2D strain tensor, angle-independent principal strains can be obtained. The two principal strains in a short-axis (SA) image slice would approximate radial and circumferential strains [5]. By visualizing strain with respect to a myocardial coordinate system, strains in different regions of a normal-functioning LV have similar magnitudes. This makes the detection of abnormal wall motion much more intuitive and brings myocardial elastography one step closer to its potential application in a routine clinical setting for reliable screening and diagnosis of myocardial disease.

II. METHODS

A. Finite-Element Analysis Model

3D finite-element analysis (FEA) models of the normal and ischemic canine left ventricle (LV) were employed to demonstrate the feasibility of the proposed elastography methods as they are currently the most comprehensive technique to model the LV [6]. These models were developed by Mazhari et al using data obtained from open-chest dog experiments before (Control) and after occlusion of the left circumflex (LCx) coronary artery [7]. The FEA files are publicly available on the UCSD Cardiac Mechanics Research Group website (<http://cmrg.ucsd.edu>). The canine LV endocardial and epicardial surfaces were fully described using a high-order bicubic Hermite interpolation scheme with a finite-element mesh consisting of 24 elements and 48 nodes (Fig. 1). The 3D rectangular Cartesian FEA models were then converted to Prolate spheroidal coordinates (λ, μ, θ) using bicubic Hermite interpolation of the radial coordinate, λ , to ensure smoothness of the endocardial and epicardial surfaces [8].

Model states were obtained at end-diastole (ED) and end-systole (ES) and linear interpolation was used to create 10 incremental model states from ED to ES. These incremental steps are not physiological but are necessary to create small displacements and small strains that could be estimated by this elastographic technique. To create 2D Short-Axis (SA) images of the LV, equatorial nodes at $\mu = 90^\circ$ were assumed to lie within the image plane as shown in Fig. 1. To simplify the model, only motion within this “image plane” is considered. With the known 2D motion of each node on the endocardium and epicardium, the 2D motion throughout the myocardial slice was calculated using bilinear interpolation.

The modeled ischemic region occupied 40% of the left-ventricular wall from base to mid level, centered about the posterior-lateral region. The end-diastolic and end-systolic pressures for both the control and LCx ischemic models were 11 mmHg and 129 mmHg, respectively. The ejection fractions (EF) for the control and LCx ischemic models were 37% and 11%, respectively.

B. 2D Ultrasonic Image Simulation

A realistic ultrasonic image was generated by convolving a 2D scatterer distribution with a 2D point spread function. The point spread function was created to simulate the impulse response of the ultrasound system with a linear transducer at a center frequency of 5 MHz, 60% fractional bandwidth and 128 elements. The scatterers were assumed to be uniformly distributed at 40 per wavelength in order to simulate the speckle in the myocardium in a SA slice. The cavity was assumed to have null scattering.

With the scatterer distribution and the 2D displacement maps, ultrasonic images were generated for all incremental time phases during the simulated contraction. As with standard ultrasound images, the simulated ultrasound images were oriented so that the linear transducer was positioned at the top. Therefore axial displacement is defined along the vertical axis and lateral displacement corresponds to motion along the

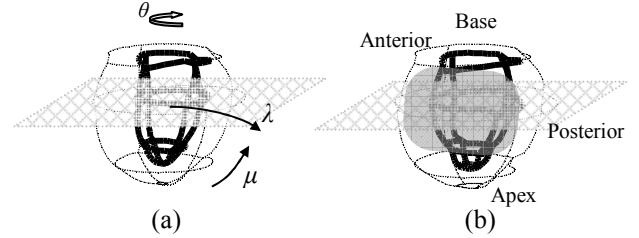


Figure 1. (a) 3D finite-element mesh for control LV and (b) for left circumflex (LCx) ischemic LV model, where (λ, μ, θ) are the prolate coordinates. In (a) and (b), solid and dotted wired mesh are the endocardium and epicardium at end-systole, respectively. In (b) the solid-gray shaded region indicates the approximate location of the ischemic region.

horizontal image axis. Each simulated B-mode image had an $80 \times 80 \text{ mm}^2$ field of view.

C. 2D Elastography

1) Displacement estimation

Cross-correlation of the RF signals was used to compute the 2D displacements between successive ultrasonic images. The technique used was similar to that described in [4]. It utilizes a 1D kernel for cross-correlation and correction in 2D for simultaneous axial and lateral motion estimation. The performance of elastography techniques in accurately estimating strains in tissues is limited to small values of strain (approximately $\pm 2\%$ strain) [9]. Therefore to create small strains, and consequently small displacements, it was necessary to use small time increments in interpolating between ED and ES. This incremental 2D motion is used to create two consecutive ultrasound images. These images are then used to iteratively estimate and correct the lateral and axial displacements.

In order to more accurately estimate lateral motion, linear interpolation was used to upsample the image in the lateral direction [4]. The accuracy of estimating the displacement in one direction is reduced even further by decorrelation due to the displacement in the orthogonal direction. To reduce the effect of this decorrelation, an iterative technique was employed to subtract the motion in one dimension before estimating the motion in the other. Once the incremental displacements were estimated, they were summed to provide an estimation of the total cumulative 2D displacement from ED to ES.

2) Strain estimation

Strain can be extracted from the displacement maps as follows. First, \mathbf{d} is defined as the 2D displacement vector for each pixel between successive image frames. It follows that the displacement gradient tensor \mathbf{G} with respect to the lateral and axial axes (x, y) is given by

$$\mathbf{G} = \nabla \mathbf{d} = \begin{bmatrix} \partial u / \partial x & \partial u / \partial y \\ \partial v / \partial x & \partial v / \partial y \end{bmatrix} \quad (1)$$

where $\mathbf{d} = u\mathbf{e}_x + v\mathbf{e}_y$. The symmetric strain tensor \mathbf{E}_{xy} , also with respect to the (x, y) axes, is derived from \mathbf{G} [5].

$$\mathbf{E}_{xy} = \frac{1}{2}(\mathbf{G} + \mathbf{G}^T + \mathbf{G}^T \mathbf{G}) \quad (2)$$

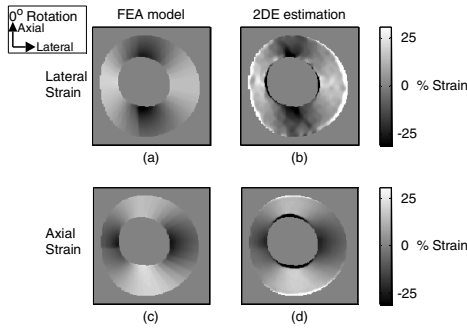


Figure 2. Control axial and lateral normal strains during contraction with transducer located to the top of image: Panels (a) and (b) are FEA and 2DE lateral strains respectively. Panels (c) and (d) show the FEA and 2DE axial strains respectively.

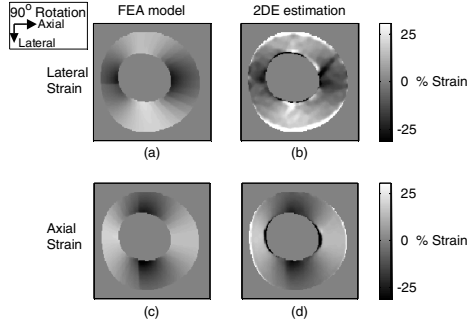


Figure 3. Control axial and lateral normal strains during contraction with the transducer located to the right of the images: Panels (a) and (b) are FEA and 2DE lateral strains respectively. Panels (c) and (d) show the FEA and 2DE axial strains respectively.

Due to the use of a gradient operator, the strain estimation was highly susceptible to noise. In order to improve the signal-to-noise ratio (SNR) in these 2D elastograms, a least-squares strain estimator (LSQSE) [10] with a 1D kernel was used. The LSQSE reduces the noise from the gradient operation through a piecewise linear curve fit to the displacement. In the case of lateral estimation, given the associated lower precision, cubic polynomial fitting was applied to smooth the lateral displacement before calculating the gradients by LSQSE [11].

D. Principal strains

Axial and lateral strains by definition are dependent on the orientation and location of the ultrasound transducer. This angle-dependence leads to the inconsistency of the strain values in the heart. Strain values in the same region of the heart will vary with the orientation of the transducer. Observe the difference in axial and lateral normal strains with the transducer at 0° and 90° rotation in Figs. 2 and 3 respectively.

Principal strains are defined as normal strains along axes of deformation where the shear strains are zero. Principal strains have been shown by Waldman et al. to be good approximations of measured radial, circumferential, and longitudinal normal strains in the myocardium [5]. Since the data and motion being considered here are only in two dimensions, only two principal strains are obtained to approximate strain in the radial and circumferential directions.

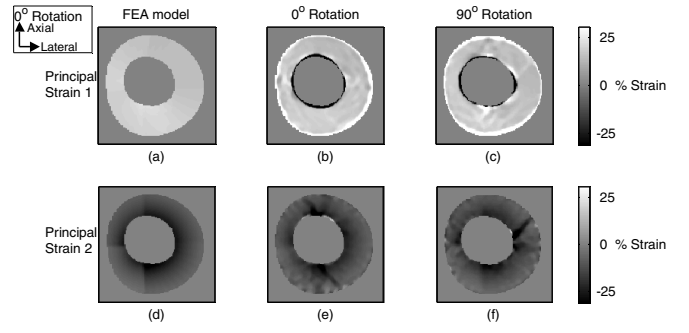


Figure 4. Control principal strains during contraction: Panels (a) and (d) show FEA model strains. Panels (b) and (e) show 2DE principal strains with transducer at top of the panels. Panels (c) and (f) show 2DE principal strains with transducer at right of the panels. Lighter areas indicate thickening strain in the myocardium, while dark areas indicated shortening strain.

With the symmetric strain tensor previously obtained, decomposing this tensor into principal strains is done by solving the algebraic eigenvalue problem, yielding the principal strains (eigenvalues) and the directions of principal axes of deformation (eigenvectors). When the principal strains are obtained they are arbitrarily sorted according to their magnitude ($E_1 > E_2$). For our purposes, the principal strains were classified as either radial or circumferential. To do this, rough estimates of radial and circumferential strains were obtained by defining θ about a manually-selected centroid and transforming the strain tensor \mathbf{E}_{xy} into radial and circumferential coordinates (\mathbf{E}_{rc}) with transformation matrix M .

$$\mathbf{E}_{rc} = M^T \mathbf{E}_{xy} M \quad \text{where} \quad M = \begin{bmatrix} \cos \theta & \sin \theta \\ -\sin \theta & \cos \theta \end{bmatrix} \quad (3)$$

Principal strain 1 was classified as that which was closer in value to the estimated radial strain and principal strain 2 was closer to circumferential.

III. RESULTS

A. 2D Elastography

Quantitative measurements show the improvement of displacement estimation between iterative corrections. The rms error of the estimated cumulative lateral displacement compared to the lateral displacement in the FEA model decreased from the first iteration to the second iteration (0.28 mm to 0.18 mm). The axial displacement rms error between model and estimate decreased from 0.118 mm to 0.117 mm.

B. Principal Strains

It is clear from observing the difference in the axial and lateral strains for the 0° and 90° rotated transducers in Figs. 2 and 3 respectively that these strain values are dependent on the angle of insonation despite the fact that the actual model deformation was identical. This is due to the altered reference coordinate system. Fig. 4 shows the FEA model principal strains alongside the 2D elastography (2DE) estimated principal strains at the 0° and 90° positions. Principal strain 1 approximates the radial strain, with light gray indicating a thickening radial strain during contraction. Principal strain 2

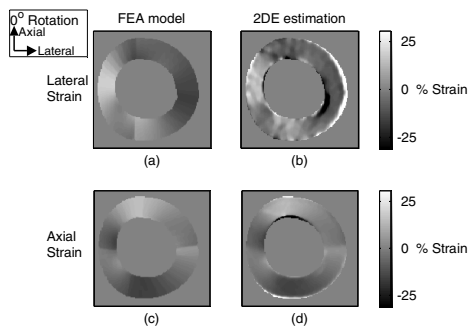


Figure 5. LCx axial and lateral normal strains during contraction. The ischemic region is in lower right quadrant. Panels (a) and (b) are FEA and 2DE lateral strains respectively. (c) and (d) show the FEA and 2DE axial strains respectively.

approximates the circumferential strain, with dark gray indicating circumferential shortening during contraction.

The estimated 2DE principal strains appear to be similar both to each other and to the FEA model principal strains (Fig 4). The rms errors between the FEA and both 2DE estimates of principal strain 1 were 1.7% and 2.4% strain, respectively. The rms error between the two 2DE estimates of principal strain 1 was 3.1% strain.

C. Control and LCx ischemic models

LCx ischemic axial and lateral strains for both FEA-model and 2DE estimated are shown in Fig. 5. Determining and quantifying the ischemic region with the strain maps shown is difficult even when the location of the ischemic region is known. Principal strains for the same model are shown in Fig 6. In contrast to the normal pattern of contraction, Fig. 6 shows abnormal deformation in the lower right of the LV with radial thinning instead of thickening and circumferential stretching instead of shortening. When the LCx principal strains are compared to those from the control model (Fig. 4), the region of abnormal wall deformation stands out clearly as being in the posterior-lateral region (lower right quadrant). This observation is consistent with occlusion of the LCx artery, as prescribed in the model.

IV. CONCLUSIONS

The iterative correction and ED-to-ES sum method successfully estimated the axial and lateral displacement images from ED to ES by accurately recreating the FEA solutions. The displacement gradients were used to obtain strains with respect to arbitrary transducer axes. Principal strains were shown to be angle-independent and were shown to be more accurate indicators of abnormal wall deformation than the axial and lateral strains. In conclusion, the feasibility of angle-independent myocardial elastography was demonstrated on a theoretical model that could render this technique highly useful for its application in a clinical setting. Future studies will focus on the in vivo application of the method described.

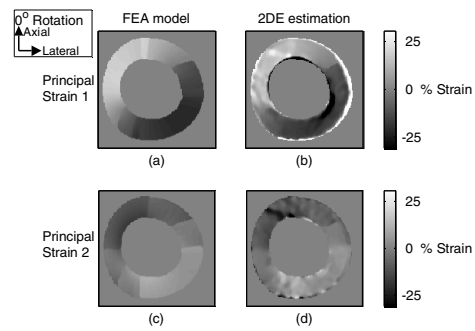


Figure 6. LCx principal strains during contraction. The ischemic region is in lower right quadrant. Panels (a) and (b) are FEA and 2DE principal strain 1 respectively. (c) and (d) show the FEA and 2DE principal strain 2 respectively. Lighter areas indicate thickening strain in the myocardium, while dark areas indicated shortening strain.

ACKNOWLEDGMENT

The authors would like to thank Dr Andrew McCulloch at the University of California, San Diego, for providing the finite element software Continuity through the National Biomedical Computation Resource (NIH P41RR08605).

REFERENCES

- [1] E. E. Konofagou et al., "Myocardial elastography- a feasibility study in vivo", *Ultrasound in Med. & Biol.*, vol. 28(4), pp. 475-482, 2002.
- [2] Meunier J. et al., "A model for dynamic texture analysis in two-dimensional echocardiograms of the myocardium", *SPIE*, vol. 768, pp.193-200, 1987.
- [3] D'hooge et al., "Two-dimensional strain rate measurement of the human heart in vivo", *IEEE Trans. Ultrason., Ferroelect., Freq. Contr.*, vol. 49, pp. 281-286, 2002.
- [4] E. E. Konofagou, and J. Ophir, "A new elastographic method for estimation and imaging of lateral displacements, lateral strains, corrected axial strains and poisons ratios in tissues", *Ultrasound in Med. & Biol.*, vol. 24(8), pp. 1183-1199, 1998.
- [5] L.K. Waldman et al., "Transmural myocardial deformation in the canine left ventricle", *Circ. Res.* vol. 57(1), pp. 152-163, 1985.
- [6] K. D. Costa et al., "A three-dimensional finite element method for large elastic deformations of ventricular myocardium--II: prolate spheroidal coordinates", *ASME J Biomech Eng.* vol. 118, pp. 464-472, 1996.
- [7] R. Mazhari et al., "Structural basis of regional dysfunction in acutely ischemic myocardium", *Cardiovasc. Res.* vol. 47(2), pp. 284-293, 2000.
- [8] A. R. Hashima et al., "Nonhomogeneous analysis of epicardial strain distributions during acute myocardial ischemia in the dog", *J. Biomechanics*, vol. 26(1), pp. 19-35, 1993.
- [9] T. Varghese and J. Ophir, "A theoretical framework for performance characterization of Elastography: The strain filter", *IEEE Trans. Ultrason., Ferroelect., Freq. Contr.*, vol. 44(1), pp. 164-172, 1997.
- [10] F. Kallel and J. Ophir, "A Least-Squares strain estimator for Elastography", *Ultrasonic Imaging*, vol. 19, pp. 195-208, 1997.
- [11] E. E. Konofagou et al., "Theoretical Bounds on the Estimation of Transverse Displacement, Transverse Strain and Poisson's Ratio in Elastography", *Ultrasonic Imaging* 22(3), 153-177, 2000.